Micromachined Planar Inductors on Silicon Wafers for MEMS Applications

Chong H. Ahn, *Member, IEEE*, and Mark G. Allen, *Member, IEEE*

***Abstract*— This paper describes three micromachined planar inductors (a spiral type, a solenoid type, and a toroidal meander type) with electroplated nickel–iron permalloy cores which have been realized on a silicon wafer using micromachining techniques. The electrical properties among the fabricated inductors are compared and the related fabrication issues are discussed, with emphasis on the low-temperature CMOS-compatible process, the high current-carrying capacity, the high magnetic flux density, the closed magnetic circuits, and the low product cost. The micromachined on-chip inductors can be applied for magnetic microelectromechanical systems devices, such as micromotors, microactuators, microsensors, and integrated power converters, which envisages new micropower magnetics on a chip with integrated circuits.**

***Index Terms*— Integrated inductor, magnetic microactuator, magnetic microelectromechanical systems, magnetic microsensor, micromachining technique, planar inductor, solenoid inductor, spiral inductor, toroidal meander inductor.**

I. Introduction

IN RECENT years, the demands for new planar micromachined inductors on "a chip" which have high inductance and Q factor have been greatly increased due to the rapid growth of magnetic driving microelectromechanical systems (MEMS) applications, such as magnetic microactuators and microsensors [1]–[8] and integrated magnetic micropower converter devices [9]–[11]. In particular, they are usually required to have high current-carrying capacity, high magnetic flux density, closed magnetic circuits, and low product cost. The fabrication of the inductive structures in a planar geometry has been understood to be an extremely difficult task, which has been the major obstacle in the implementation of fully integrated and miniaturized magnetic MEMS devices.

Applications of these inductive components have usually been limited due to the relatively low inductance which can be achieved, typically on the order of hundreds of nanohenries to several microhenries. Thus, most previously fabricated structures have been operated in very-high-frequency regimes, for instance, as passive components in microwave circuits, as well as signal processing circuits [12]–[18]. Although several inductive thin-film heads [19]–[21] have been successfully realized for magnetic disk drive systems, the inductive components have also been investigated in focusing not on micropower applications, but for signal processing with extremely low noise.

Thus, conventional planar inductors realized to date are usually optimized not for their achievable maximum powers, but for their maximum operating frequencies. However, in recent years, there is a major need for the development of miniaturized planar inductors implemented on "a chip" as a strong magnetic flux generator to produce strong forces for MEMS microactuators, as well as to contain large energy for micropower converters. In the micro scale, magnetic driving principle has been considered as one of the most promising principles to produce a large force, since it potentially can overcome the drawbacks which would be caused by other driving principles, depending on application areas and scales [1]–[8].

To date, several different types of planar inductors have been proposed and fabricated to address these applications [12]–[18]. However, most planar inductive components have been fabricated without using a completely closed magnetic circuit, so that leakage flux from the inductor is not negligible. This can be a serious problem in integrating inductors with electronic circuits on the same semiconductor wafers for two reasons. First, magnetic flux interference with an integrated electronic circuit should be suppressed to reduce the magnetic noise in the circuits, and second, a high inductance per unit surface area is desirable in the small area, and any leakage flux produced does not contribute to the total inductance of the device.

Recently, new micromachining magnetic MEMS techniques [1]–[8] have been developed, which shows a promise to revolutionize the conventional concepts of magnetic microstructures. These micromachining techniques provide several approaches for miniaturization of magnetic power components. Cores and conductors of several tens to hundreds of micrometers in thickness and width with good sidewall and dimensional control can be easily fabricated. Recently, three new types of micromachined planar inductive components with closed magnetic circuits, a spiral type [23], a solenoid type [24], and a toroidal-meander-type inductor [25], have been realized on silicon wafers with electroplated nickel–iron permalloy [26]–[28] using the micromachining techniques. In particular, emphasis is placed on low-temperature CMOS-

Manuscript received March 5, 1997; revised August 25, 1998. Abstract published on the Internet August 25, 1998. This work was supported in part by the National Science Foundation under Grant ECS-9117074.

C. H. Ahn was with the Microelectronics Research Center, School of Electrical and Computer Engineering, Georgia Institute of Technology, Atlanta, GA 30322-0250 USA. He is now with the Center for Microelectronic Sensors and MEMS, Department of Electrical and Computer Engineering and Computer Science, University of Cincinnati, Cincinnati, OH 45221-0030 USA.

M. G. Allen is with the Microelectronics Research Center, School of Electrical and Computer Engineering, Georgia Institute of Technology, Atlanta, GA 30322-0250 USA.

Publisher Item Identifier S 0278-0046(98)08460-3.

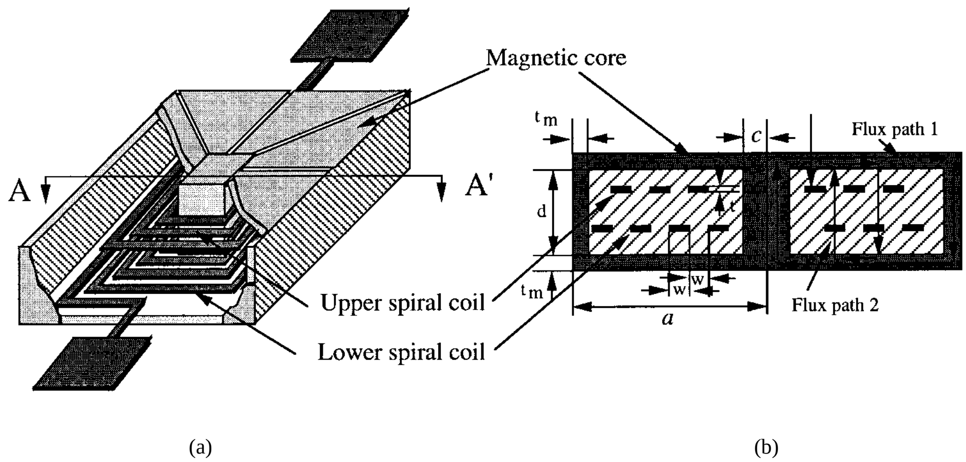

Fig. 1. Spiral-type inductive structure. (a) Schematic diagram which has a closed magnetic circuit and (b) simulation model.

compatible fabrication, high current-carrying capacity of the fabricated inductive components, high magnetic flux density, closed magnetic circuits, and low product cost.

In magnetic microactuator applications, the magnetic reluctance in a small air gap which is inserted into the closed magnetic circuit is usually comparable to the magnetic core reluctance, or negligibly small [29]. Thus, the air gap inserted into the core may not break the tight flux linkage between the coils and the magnetic circuits, keeping the minimum electromagnetic field interference (EMI).

In this paper, the electrical characteristics of the three micromachined inductors are compared in terms of inductance, conductor resistance, and Q factor. Their geometrical effects on electrical properties are also analyzed, and then their potential MEMS applications are discussed, depending on their structural, as well as electrical, characteristics.

II. Structure Concepts and Models

A. Spiral-Type Inductor

Several planar spiral inductors have already been reported to date. In these inductors, spiral conductors are placed on an insulated substrate [12]–[14], a magnetic substrate [15], or between top and bottom magnetic thin films [16]. Due to the geometrical characteristics of the spiral, the generated fluxes without magnetic cores will be spread throughout the surface of the substrate. These fluxes are composed of two components which are either parallel or perpendicular to the surface [14]. Accordingly, it is difficult to guide the magnetic flux to a required point in this structure without using a magnetic core. As one of the applications of these inductors, integrated magnetic recording heads have been investigated since the early 1970's. In the magnetic heads, a stack of spiral conductors is deposited on the bottom magnetic core layer, and then top magnetic layers are successively deposited to build magnetic legs, completing a closed magnetic circuit through the gaps [19]–[22]. However, the magnetic heads have been optimized for nonactuator applications, and they may not have high flux generation capability and/or large current-carrying capability required for magnetic microactuators. Thus, for magnetic micropower application, a new spiral-type inductor which is composed of completely closed magnetic circuits and thick conductor lines is introduced.

There are two major restrictions that must be overcome to improve the usefulness of this geometry in micropower applications. First, closed magnetic circuits should be completed using a thick magnetic material with high permeability to reduce magnetic reluctance and to minimize magnetic field interference (making the adhesion of the thick magnetic layer a concern). Second, the spiral conductor should have as small a resistance as possible to reduce power consumption in the conductors. To overcome these limitations, micromachining fabrication techniques are used to build a spiral-type inductive component that is composed of completely closed magnetic circuits and thick conductor lines. The spiral inductor structure for this paper is shown in Fig. 1(a), where spiral conductor lines are completely encapsulated with an electroplated thick nickel–iron permalloy, thus achieving the closed magnetic circuit.

Simplified models of double spiral coils for the inductance calculation of the closed outer core have been developed [9], [13]. Fig. 1(b) shows a schematic diagram of the inductor which is to be modeled to determine its inductance value. To calculate the mutual inductance, three components of inductance which exists between the ith and jth coils can be defined. If the inductances for path 1, path 2, and internal self-inductance of the coil are defined as L_1, L_2, and L_i, respectively, the total inductance L obtained from the summation of these inductances is

$$L = L_1 + L_2 + L_i. \tag{1}$$

To evaluate an inductance of the spiral-type inductor, designed micromachining geometries are substituted into the model. For $a = 1346$ μm, $c = 508$ μm, $d = 30$ μm, $N = 18.5$, $t_m = 8$ μm, and $w = 12.5$ μm, the evaluated values are $L_1 = 14.5$ μH, $L_2 = 10.2$ μH, $L_i = 0.01$ μH, and $L = 24.71$ μH, respectively, where a relative permeability of 800 is assumed. From these calculated values, it is interesting to note that the inductance value resulting from path 2 including the air gaps has an almost comparable value to the inductance value resulting from path 1 through the closed magnetic circuits.

The Q factor of this inductor can be expressed with the spiral conductor resistance of R as

$$Q = \frac{\omega L}{R}. \quad (2)$$

When the thickness of the conductor lines is increased, the conductor resistance will be reduced. Also, L_1 and L_2 are not greatly affected by the gap variation between the upper core and the lower core which results from the variation of conductor thickness. As a result, the increase in Q factor resulting from increasing the conductor thickness will be mainly caused by the decrease in the conductor resistance. Thus, the Q factor increases almost linearly as the thickness of the conductor is increased.

When a planar inductive component is fabricated monolithically with integrated circuits, the area occupied by the planar inductive component must be limited. In a given area (i.e., for the given length of a in this model), the spiral coil turns and resistance are varied as the conductor width (w) is changed. The dimension of the center magnetic core (i.e., defined as c in this model) also affects the available area which can be occupied by the conductors. Using (1) and (2), Q factors can be evaluated by changing for the fixed area. It is verified from this evaluation that the Q factor has larger values in smaller conductor widths, where the inductance value is proportional to the square of the coil turns (i.e., the square of the width variation), but the resistance is linearly proportional to the width variation.

B. Solenoid-Type Inductor

Conventional inductors used in macro scale usually have a solenoid shape and, thus, they can be simply fabricated by wrapping coils manually around magnetic cores at macro scale. However, this three-dimensional winding structure causes a tremendous difficulty in realizing in planar shape on a wafer. To demonstrate the feasibility of a planar solenoid inductor, solenoid inductive components were fabricated in a hybrid fashion by manually wrapping coils around a magnetic film [30] or an integrated fashion by wrapping coils around an air core on a silicon substrate [31]. However, the fabrication processes and/or the obtained electrical parameters are not suitable for integrated micromagnetic power device applications. In this paper, thus, a new technique is adopted to overcome these limitations using planarization with polyimides and inserting a magnetic bar core in place of the air core. To fabricate this inductor on a planar substrate, quasi-three-dimensional micromachining techniques which are compatible with IC processes are required. This planar solenoid-type inductor with a closed magnetic circuit can be one of the favorable structure as a magnetic flux generator in micro scale, since the wires wrapped around closed magnetic cores result in low leakage flux and the generated flux can be flexibly guided to the required points. In this paper, such structures have been fabricated using multilevel metal schemes to "wrap" a wire around a magnetic core.

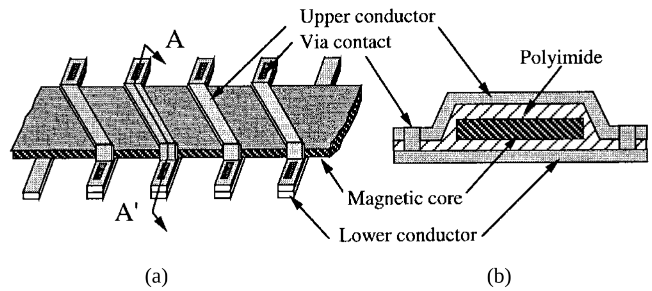

Fig. 2. Schematic diagram of the solenoid-type inductive component: (a) schematic view and (b) A–A' cut view.

The proposed solenoid-type inductor structure is depicted in Fig. 2, where the geometry can be thought of as analogous to the conventional toroidal inductor. In this structure, the interconnected metal coils wrap around the magnetic core bar. This type inductive component is considered as one of the more promising inductive components for magnetic micropower device applications, since its geometrical characteristics can meet most of the required conditions of a basic inductive component for magnetic MEMS applications [29].

The metal interconnections used to construct the "wrapping coils" usually include metal via contacts. These via contacts are another obstacle in the practical applications of this component since they may have a relatively high contact resistance which causes a specific heat dissipation in the via contacts. In achieving a high inductance value, if more turns of solenoid coils are required, more via contacts are added, increasing the total coil resistance. Evaporated metal deposition techniques limit the achievable thickness of a deposited metal and usually cause a high metal contact resistance at the via contacts due to metal oxide or surface contamination resulting from subsequent fabrication processes [33]. As a result, when a high current is applied to the conductor coils, heat is generated locally at the via contacts due to their high resistance, resulting in a potential instability problem in this inductive component. Using electroplating techniques, particular efforts have been made to minimize the coil resistance by increasing the thickness of the conductor lines and using electroplated vias. An additional feature of this inductor is that a closed (i.e., toroidal) magnetic circuit is achieved, minimizing the leakage flux and electromagnetic interference and increasing the inductance value and the Q factor.

The geometry of the solenoid-type inductor depicted in Fig. 2 can be analogous to the conventional toroidal inductor. Thus, the calculation of the inductance of a solenoid-type structure is very simple and more or less straightforward. The inductance L of the solenoid inductor structure is expressed as

$$L = \frac{\mu_0 \mu_r N^2 A_c}{l_c} \quad (3)$$

where A_c is the cross-sectional area of the magnetic core, l_c is the length of the closed magnetic core, and μ_0 and μ_r are the permeability of the vacuum and the relative permeability of the magnetic core, respectively. To evaluate an inductance of the designed inductor shown in Fig. 2, the designed geometries and the measured permeability are substituted into (3). For

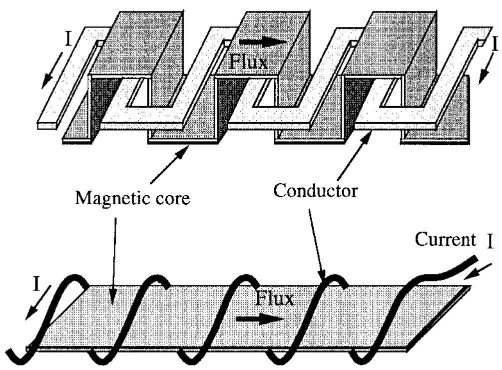

Fig. 3. Schematic diagrams of the toroidal-meander-type inductor. The structure of the two inductor schemes is analogous: (a) toroidal-meander-type inductor and (b) solenoid type inductor.

$A_c = 300\ \mu\text{m} \times 20\ \mu\text{m}$, $l_c = 9000\ \mu\text{m}$, $N = 33$ turns, and $\mu_r = 800$, the evaluated inductance value is 0.729 μH.

The Q factor of the inductor can be expressed as

$$Q = \frac{\omega_L}{R} = \frac{\omega\mu_0\mu_r N A_c A_w}{2W\rho l_c} \tag{4}$$

where A_w is the cross-sectional area of the conductor, $2W$ is the length of coil per turn, and ρ is the resistivity of the conductor material.

From (3) and (4), it is concluded that inductance and Q factor are linearly proportional to μ_r in the solenoid-type inductor, as well as the conventional toroidal inductor, due to the analogous structure of both inductors.

C. Toroidal-Meander-Type Inductor

In the solenoid-type inductor, the conductor lines are wrapped around a magnetic core to form an inductive component. However, by interchanging the roles of the conductor wire and magnetic core in the solenoid inductor, the same effect can be achieved, i.e., a multilevel magnetic core is "wrapped" around a planar conductor. A new integrated toroidal-meander-type inductor can be realized, where toroidal refers to the toroidal core geometry and meander refers to the wrapping approach. This structure has the advantage that a relatively short, planar conductor is used, thus reducing the total conductor resistance. In addition, this geometry has an advantage over the other inductors in realizing microactuators, since the magnetic core is produced on two levels, making it readily available for surface micromachining of movable core actuators.

A schematic drawing of a section of the new integrated toroidal-meander-type inductor is shown in Fig. 3. This inductor geometry is composed of meander conductor lines located on a simple plane and meander magnetic cores located on the multilevels. Since multilevel meander magnetic cores are interlaced through the center of each meander coil, the magnetic flux density at the center of each meander coil can be calculated by evaluating magnetic fields at the center points, which are generated from the current flowing through all meander conductor elements, as shown in Fig. 4(a).

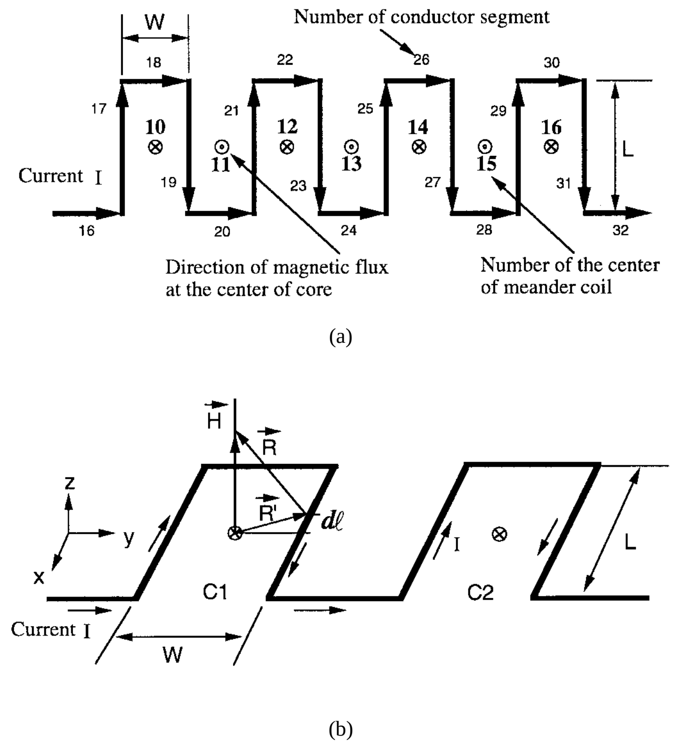

Fig. 4. Meander conductor models: (a) coordinate and meander elements for the Biot–Savart law calculation and (b) model of meander conductor including the direction of magnetic flux.

By expanding this topology to all distributed meander conductor elements, as shown in Fig. 4(b), the inductance can be calculated from the total flux linkage (both self and mutual flux linkage) as

$$L = \frac{\Sigma\Lambda}{I} \tag{5}$$

where $\Sigma\Lambda$ denotes the total flux linkage, which occurs between the closed multilevel meander magnetic circuit and the flux generated from the current flowing through all meander conductor elements. Note that this relation assumes that the material remains magnetically linear. The z components of the distributed magnetic flux at these centers are shown in Fig. 5. Although, at the center of each meander coil the vector direction of the z component of the magnetic flux varies from point to point in the opposite direction, all fluxes of z component in the magnetic circuit flow constructively through the multilevel meander core due to the core geometry. The dimensions of the fully fabricated toroidal-meander-type inductor shown in Fig. 4 are as follows: the total inductor size is 4 mm $\times$ 1.0 mm; the coil has 30 turns; μ_r is 800; and the cross-sectional areas of the magnetic core and the conductor coil are $300\ \mu\text{m} \times 12\ \mu\text{m}$ and $50\ \mu\text{m} \times 7\ \mu\text{m}$, respectively. The inductance evaluated from (5) is 0.22 μH.

The Q factor of an inductor can be expressed as

$$Q = \frac{\omega L}{R} = \frac{\omega\mu_0\mu_r N A_c A_w}{2(W+L)\rho l_c} \tag{6}$$

where A_w is the cross section area of conductor, $2(W + L)$ is the length of one meander coil turn, and ρ is the

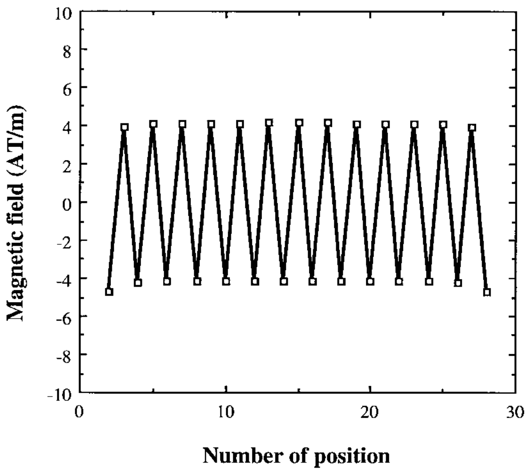

Fig. 5. Magnetic field distributions at the center of each meander coil with an assumed current of 1 mA flowing through the conductors. The positive and the negative signs of magnetic field indicate the directions of magnetic field at Z axis.

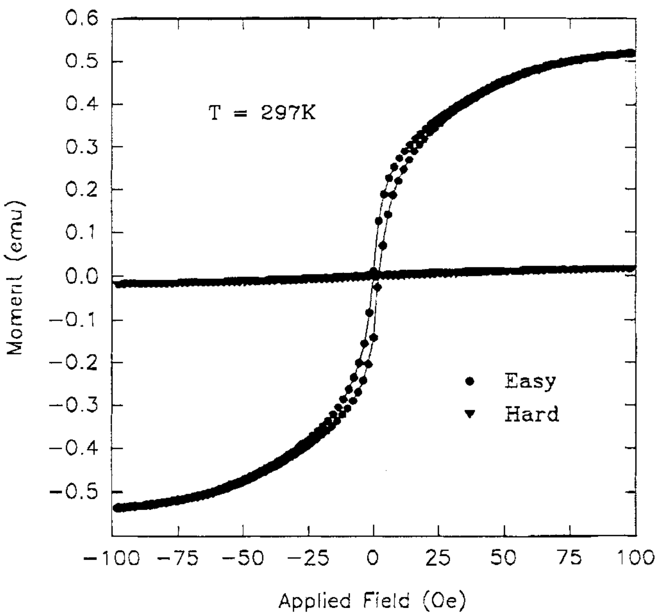

Fig. 6. A *B–H* curve of the electroplated nickel (81%)–iron (19%) permalloy.

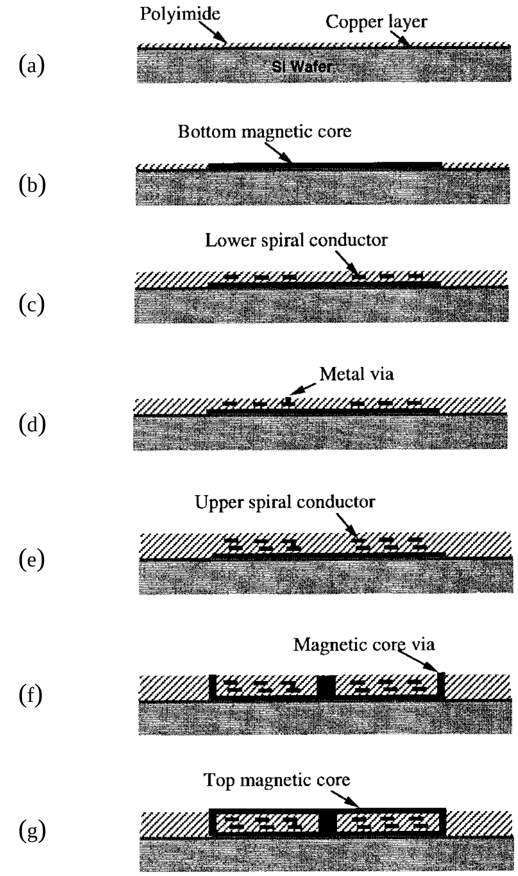

Fig. 7. Fabrication sequence of the planar-spiral inductive component.

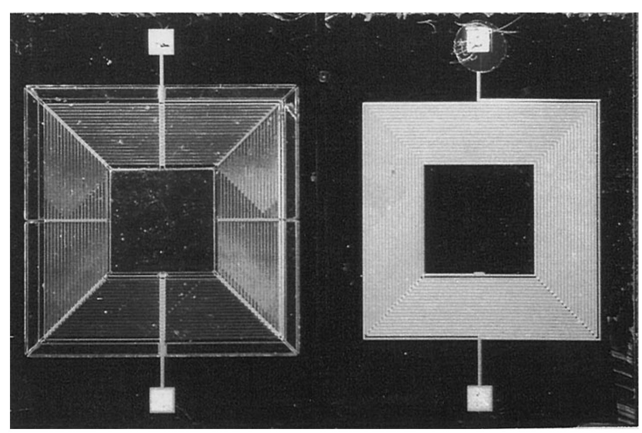

Fig. 8. Photomicrograph of the inductive components with (left side) or without (right side) a magnetic core.

resistivity of conductor material. From (3)–(6), it is concluded that inductance and Q factor are linearly proportional to μ_r in the solenoid-type inductor, as well as in the toroidal-meander-type inductor, due to the analogous structure in both inductors. Thus, the introduction of thin-film magnetic core in the integrated inductors greatly improves the inductance, as well as the Q factor.

III. Fabrication

These three inductive components have very similar fabrication steps. Fabrication process started with oxidized (0.6 μm) 3-in $\{100\}$ silicon wafers as a substrate. Onto this substrate, chrome–copper–chrome (300 Å/2000 Å/300Å) was deposited as an electroplating seed layer. In this fabrication, polyimide, which is known as a good passivation organic material for integrated circuits, was used as a basic insulator, a device molder, and a structure holder, because it has good insulating properties, as well as good planarization and mechanical properties. Relative permittivity of polyimide is approximately 3.0, which is a very similar value to that of silicon oxide. Thick copper or aluminum conductors are plated or deposited, and nickel (81%)–iron (19%) permalloy cores are plated through the defined molds using standard electroplating technique [26], [34], [35]. A *B–H* curve of the electroplated nickel (81%)–iron (19%) permalloy is plotted in Fig. 6.

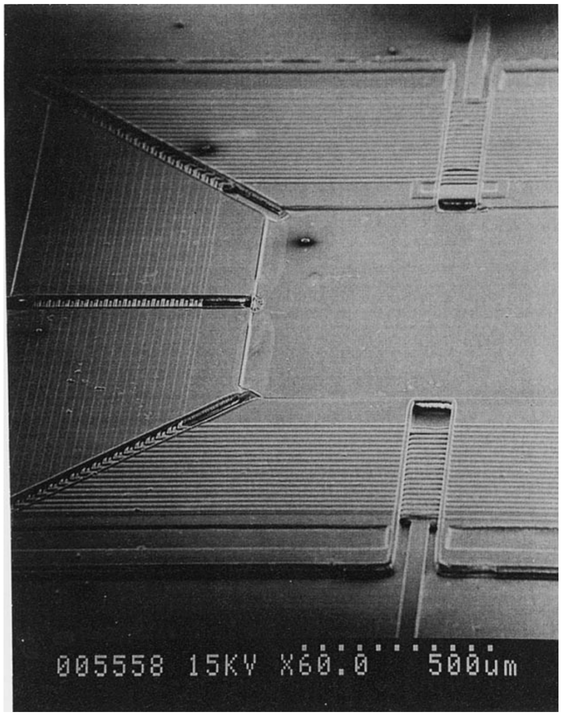

Fig. 9. Scanning electron micrograph of the fabricated spiral-type inductor.

The fabrication steps of the spiral inductor are shown in Fig. 7. Polyimide was spun and cured on the wafer to build electroplating molds for the bottom magnetic core. Holes were dry etched in this polyimide and then filled with the nickel–iron permalloy using standard electroplating techniques. For the lower spiral conductor, aluminum was deposited onto the polyimide and patterned using conventional lithography. In order to insulate the conductor line and re-planarize the surface, polyimide was deposited in multiple coats. To connect the lower spiral coils to the upper spiral coils, a via hole was then dry etched through the polyimide layer. Aluminum or copper was deposited and patterned again for the via and upper spiral coils, composing a double-layer spiral conductor. To complete a closed magnetic circuit, magnetic vias were etched both at the center and at the outside of the spiral coils. The magnetic vias were filled with plated nickel–iron permalloy. The top magnetic core was then plated over the magnetic vias, completing the magnetic circuit. Bonding pads were then opened through polyimide layers for the electrical test. The fabricated spiral-type inductor has the size of 3 mm $\times$ 3 mm $\times$ 150 μm, having 36 turns of spiral coil. The photomicrograph of the fabricated spiral inductive components with or without an encapsulating magnetic core are shown in Fig. 8. Fig. 9 shows a scanning electron micrograph of the fabricated spiral inductor.

The brief fabrication processes of the solenoid-type inductor are shown in Fig. 10. The seed layer for bottom conductors was patterned to form the tie bars to be removed after serving as the seed layer for the conductor plating. The cavity to contain the magnetic core bar was dry etched. The copper conductors and nickel–iron permalloy were plated through the defined molds using standard electroplating techniques. Most fabrication procedures are very similar to those of the spiral-type inductor, except the electroplated conductors. Fig. 11 shows the photomicrograph of the fully fabricated device. The size of fabricated structure is 4 mm $\times$ 1.0 mm $\times$ 120 μm, having 33 turns of multilevel coils. The scanning electron micrograph of the structure is shown in Fig. 12, which was taken after dry etching of the polyimide.

The fabrication processes of the toroidal-meander-type inductor is also depicted in Fig. 13. This meander geometry has

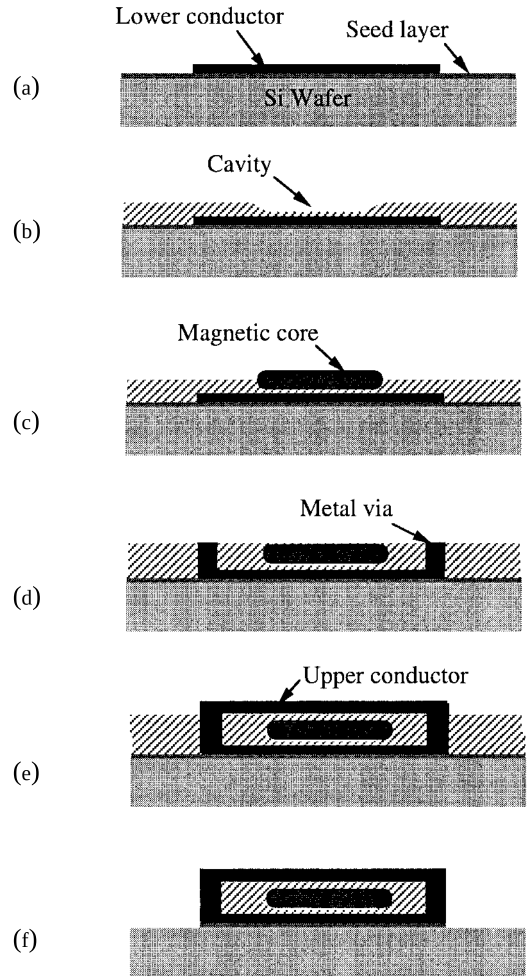

Fig. 10. Fabrication steps of the solenoid-type inductive component.

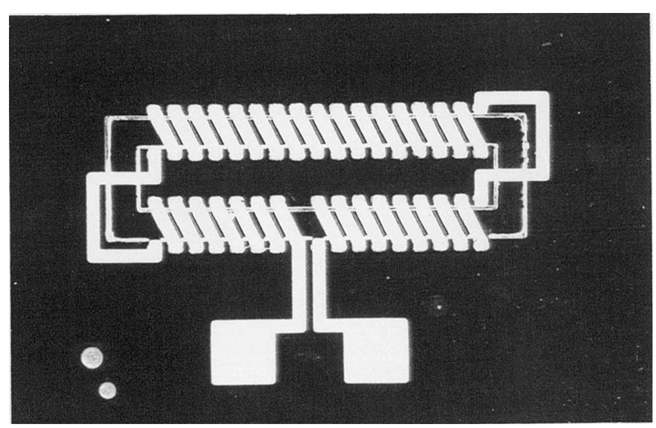

Fig. 11. Photomicrograph of the fabricated solenoid-type inductor.

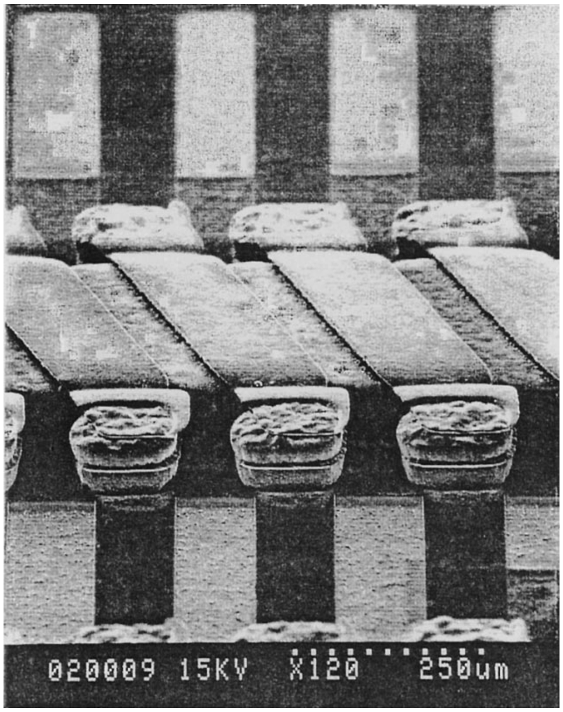

Fig. 12. Scanning electron micrograph of the fabricated solenoid-type inductor.

no electrical vias that add resistance to the conductor coil, since the conductor is located in a single plane. Most fabrication procedures are also very similar to the spiral type, as well as the solenoid-type inductor. The fabricated inductor size is 4 mm $\times$ 1.0 mm $\times$ 130 μm, which has 30 turns. Fig. 14 shows scanning electron micrographs of the fabricated toroidal- and meander-type inductor. Note the magnetic via connecting the top and bottom cores in the meander topology.

Finally, all samples were diced into chips for bonding and test.

IV. Device Performance and Discussion

From a typical 36-turn spiral-type inductor of 3 mm $\times$ 3 mm in area, an inductance of approximately 20 μH was measured at 10 kHz. A plot of inductance versus frequency for two planar spiral-type inductor structures, one with a magnetic core and the other without a magnetic core, is shown in Fig. 15. The magnetic core has increased the inductance by a factor of 4–5 compared with the structure without the magnetic cores. The obtained inductance of 2.2 μH/mm^2 at 10 kHz is one of the highest inductance values which has been achieved in an integrated planar inductive component, corresponding to a core permeability of approximately 800. It should be noted that the increase in inductance falls off at frequencies above 3 MHz, presumably due to the decreasing permeability of the nickel–iron permalloy at higher frequencies. The evaluated inductance for this fabricated inductor was 24.71 μH. Thus, the measured and the evaluated inductances are matched well at low frequencies. The measured conductor resistance was approximately 300 Ω. The achieved Q factor at frequencies around 1 MHz is approximately 0.25. However, in realizing an actual magnetic microactuator using the spiral inductor with magnetic cores, the highest Q factor may not be as important as the lowest conductor resistance. In order to evaluate the capacitance of the inductor, an equivalent circuit was assumed, as shown in Fig. 16, and the resistance and stray capacitance of the inductor were derived from the measured impedance and phase as a function of frequency using equivalent circuit analysis. From this analysis, for a typical 36-turn device 3 mm $\times$ 3 mm inductor, the stray capacitance was shown to be in the several tens of picofarads and also shown to have a negligibly small effect over the low-frequency ranges used. If a small air gap is introduced between the top core and the center core pole, magnetic force can be generated at the air gap when a current is applied to the spiral coils. Fortunately, air gaps and movable mechanical structures can be easily inserted as part of the magnetic circuit in this structure by using surface micromachining techniques and sacrificial layers. Thus, this spiral-type inductor implemented on a chip can serve as an inductive component in realizing magnetic integrated circuits or modules, such as filters, microsensors, dc/dc converters, microvalves, and micropumps.

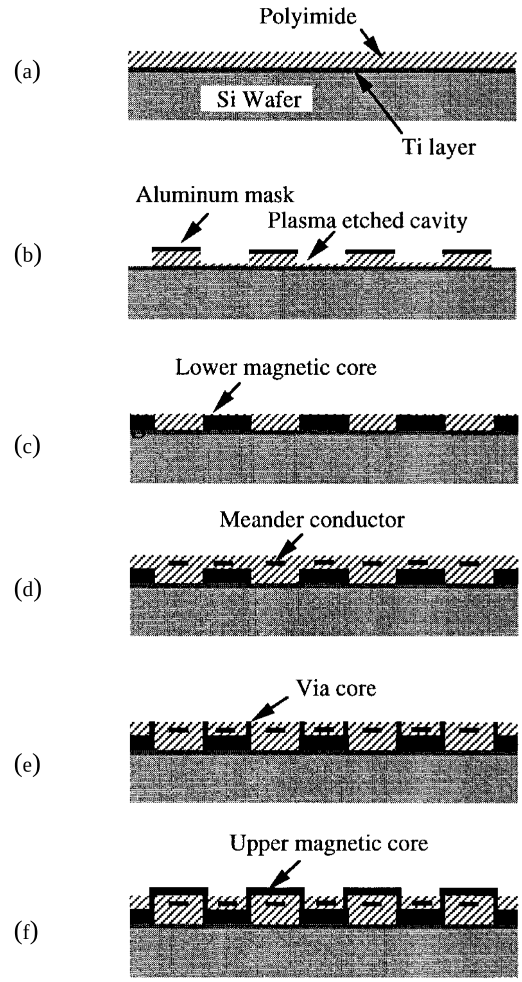

Fig. 13. Fabrication sequence of the toroidal-meander-type inductor.

For a solenoid-type inductor of 4 mm $\times$ 1.0 mm $\times$ 120 μm thickness having 33 turns of multilevel coils, the achieved inductance was approximately 0.4 μH at low frequencies of approximately 10 kHz. The variation of the inductance with

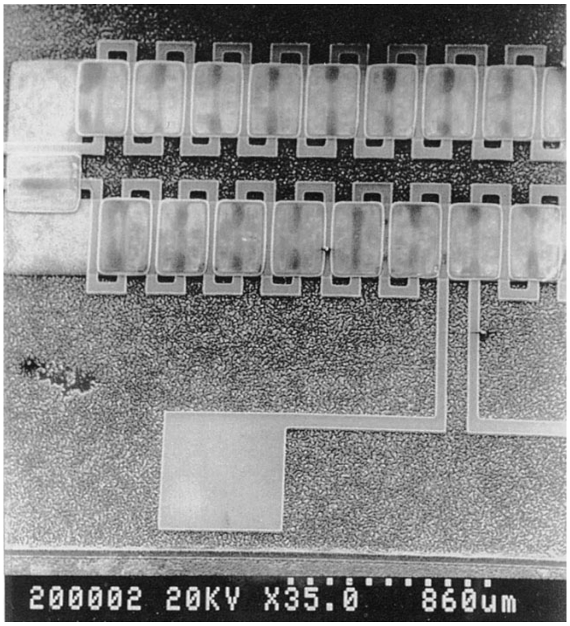

(a)

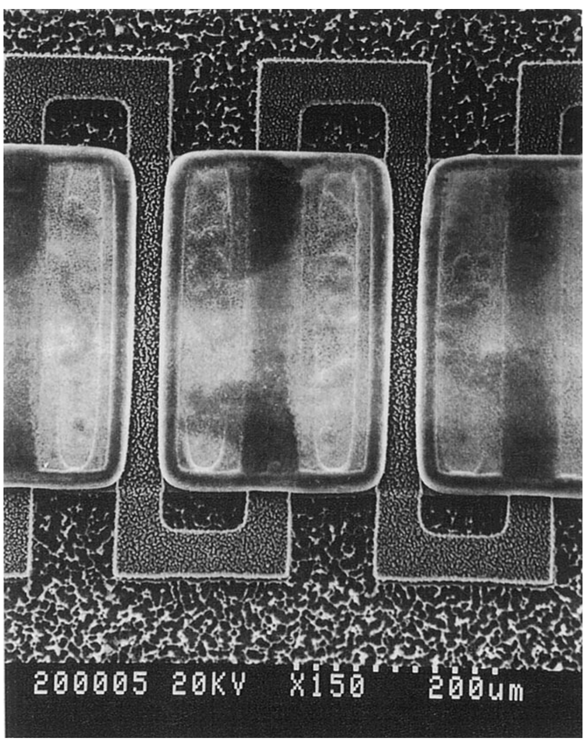

(b)

Fig. 14. Scanning electron micrograph of the fabricated toroidal-meander-type inductor. (a) Half of the inductor and (b) detailed view.

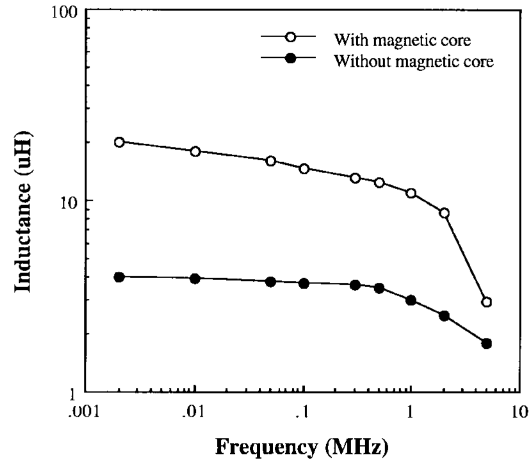

Fig. 15. Measured inductance of the spiral-type inductor.

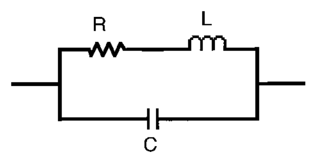

Fig. 16. Equivalent circuit of the spiral-type inductor.

frequency is shown in Fig. 17(a). As evaluated in the previous section, the evaluated inductance for this fabricated inductor was 0.729 μH. The measured and the evaluated inductances are also matched well at low frequencies. The measured resistance of the conductor lines was approximately 0.3 Ω. The conductor resistance evaluated from its geometry was approximately 0.308 Ω using a literature value for conductivity of plated copper [32]. Although it was difficult to measure a via contact resistance individually, it was verified from the comparison between the measured and the estimated values that the resistance of a metal via contact had an almost negligible value. Thus, the electroplating technique eliminated via contact instability or high contact resistance problems potentially resulting from unfavorable metal via contacts. The evaluated Q factor at 1 MHz was approximately 1.5, the relatively higher value of which compared with the spiral type would be mainly due to its low conductor resistance. The stray capacitance was shown to be in the picofarad region and, thus, it gives a negligibly small effect over the frequency ranges used. The effect of the inductance falloff at higher frequencies shown in Fig. 17(a) is due almost entirely to the dependence of the permeability of the iron–nickel core on frequency. Since this inductive component has favorable magnetic characteristics, as well as electrical properties, it is potentially very useful as a basic inductive component in applications for magnetic microsensors, micromotors, electron beam steering lenses, and micromagnetic power devices, such as a dc/dc converter.

The fabricated toroidal-meander-type inductor of 4 mm $\times$ 1.0 mm $\times$ 130 μm in size has 30 coil turns. The cross-sectional areas of the magnetic core and the conductor coil are 300 μm $\times$ 12 μm and 50 μm $\times$ 7 μm, respectively. The measured inductance values were plotted in Fig. 17(b), which shows a fairly flat response through a frequency of 10 MHz. At a frequency of 5 MHz, an inductance of 30 nH/mm^2 was achieved. The evaluated inductance for this fabricated inductor was 0.22 μH and, thus, the measured and the evaluated

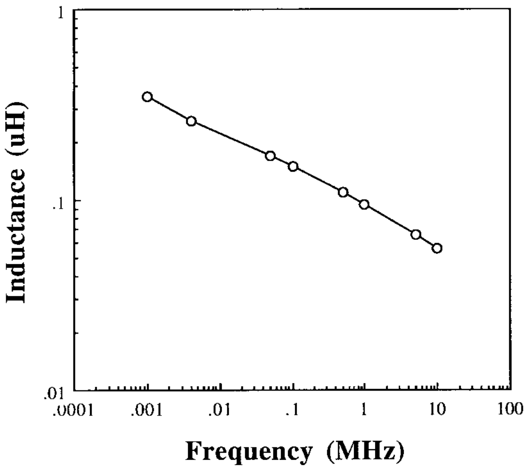

(a)

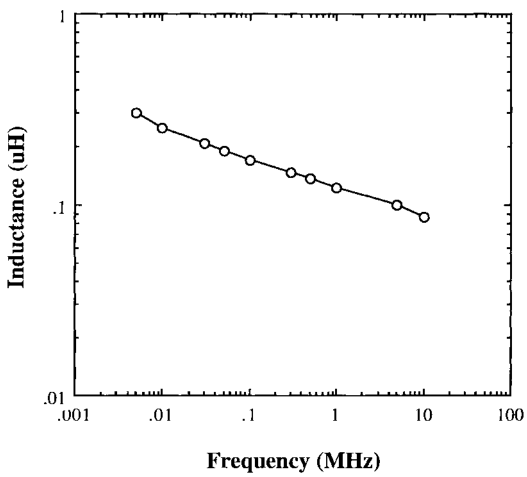

(b)

Fig. 17. Measured inductance: (a) solenoid-type inductor and (b) toroidal-meander-type inductor.

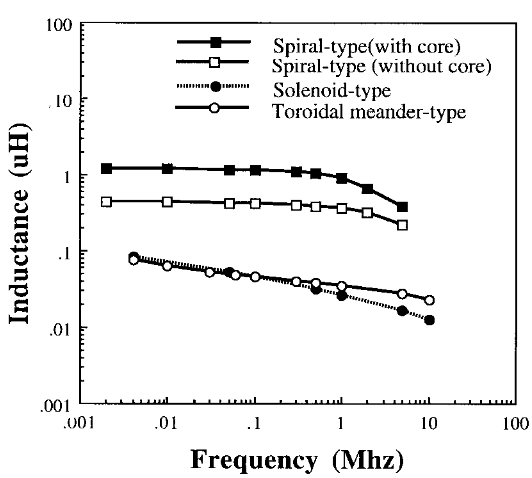

Fig. 18. Measured inductance per area (μH/mm^2) for the three micromachined inductors.

TABLE I
ELECTRICAL PARAMETERS OF THE MICROMACHINED INDUCTORS

Inductor Type	Inductance ($\mu H/mm^2$) (at 10 KHz)	Resistance (Ω/mm^2)	Capacitance (F)	Q-factor (at 1 MHz)
Spiral Type	1.3	5.6	approximately pF	0.25
Solenoid Type	0.1	0.1	approximately pF	1.5
Toroidal-Meander Type	0.05	0.06	approximately pF	1.0

inductances also show fairly good match at low frequencies. The stray capacitance was shown to be in the picofarad region. With the measured inductance and resistance as a function of frequency, the Q value of the device can be estimated from (6). The Q value at a frequency of 1 MHz is approximately unity. Several approaches, such as increased conductor thickness (to lower the series resistance) or increased core permeability, could be taken to increase the Q factor. Finally, the measured inductances for the micromachined three inductors are plotted in Fig. 18, and their electrical parameters are listed in Table I.

The toroidal-meander-type inductor implemented on a chip or as an integral part imbedded in the interconnections of a multichip module has already been used as an inductive component in realizing magnetic integrated circuits or modules, such as microactuators [36]–[38], dc/dc power converters [39], or biomedical applications [40]. When this inductor is used as an inductive component for the integrated dc/dc converter, the heat dissipation capability of the inductor will limit the maximum current flowing through the conductors. By applying dc current through the inductor coils using a Tektronix 370A programmable curve tracer, coil resistance was estimated from the slope of the V–I curve. Using the equation of resistance–temperature for the conductor, the temperature of the conductor could be calculated from the measured resistance. This calculation yields a conductor temperature of 50 °C at 250 mA. This indicates that the meander film conductor permits high current density. For instance, the maximum recommended current density of the conventional inductor [14] in the macro scale at 50 °C has been reported as 5×10^2 A/cm^2. In this inductor, it was verified that the attainable maximum current density ranged from 5×10^4 A/cm^2 to 5×10^5 A/cm^2. These values are two orders of magnitude larger than the values in the macro scale, which implies that the heat generated from the integrated inductors can be quickly dissipated from the inductors.

V. CONCLUSIONS

In this paper, three new micromachined planar inductors, a spiral, a solenoid, and a toroidal meander type, have been realized on silicon wafers using micromachining and multilevel metal fabrication techniques. Their electrical and geometrical properties are compared for magnetic MEMS applications. In particular, emphasis is placed on low-temperature CMOS-compatible process, high current-carrying capacity, high magnetic flux density, closed magnetic circuits, and low product cost. The realized inductive components have shown their suitability for magnetic micropower applications, such as magnetic micromotors, magnetic microactuators, microsensors, magnetic particle separators, and miniaturized dc/dc converters, which envisages new micropower magnetics on silicon wafers with integrated circuits.

ACKNOWLEDGMENT

The authors would like to gratefully acknowledge DuPont and OCG Microelectronic Materials for the donations of polyimide and Lake Shore Cryotronics, Inc. for assistance in measurements of the magnetic properties of the permalloy thin films. The fabrication was performed in the Microelectronics Research Center, Georgia Institute of Technology.

REFERENCES

[1] K. Yanagisawa, A. Tago, T. Ohkubo, and H. Kuwano, "Magnetic micro-actuator," in *Proc. 4th IEEE Workshop on Microelectromechnical Systems,* Nara, Japan, 1991, pp. 120–124.

[2] H. Guckel, K. J. Skrobis, T. R. Christenson, J. Klein, S. Han, B. Choi, E. G. Novell, and T. W. Chapman, "On the application of deep X-ray lithography with sacrificial layers to sensor and actuator construction," *J. Micromech. Microeng.,* vol. 1, no. 4, pp. 135–138, 1991.

[3] B. Wagner, M. Kreutzer, and W. Benecke, "Linear and rotational magnetic micromotors fabricated using silicon technology," in *Proc. IEEE Microelectromechanical Systems Workshop,* 1992, pp. 183–189.

[4] C. H. Ahn and M. G. Allen, "A fully integrated micromagnetic actuator with a multilevel meander magnetic core," in *Proc. IEEE Solid-State Sensors and Actuators Workshop,* 1992, pp. 14–18.

[5] I. J. Busch-Vishniac, "The case for magnetically driven microactuators," *Sens. Actuators,* vol. A-33, pp. 207–220, 1992.

[6] C. Liu, T. Tsao, Y. C. Tai, and C. M. Ho, "Surface micromachined magnetic actuators," in *Proc. IEEE Microelectromechanical Systems Workshop,* 1994, pp. 57–62.

[7] F. Cardot, J. Gobot, M. Bodgdanski, and F. Rudolf, "Fabrication of a magnetic transducer composed of a high-density array of micromagnets with on-chip electronics," *Sens. Actuators,* vol. A-43, pp. 11–16, 1994.

[8] R. Miller, G. Burr, Y. C. Tai, and D. Psaltis, "Magnetically actuated micromirror use as optical deflectors," in *Proc. Electrochemical Soc. Meeting,* Oct. 1995, vol. 95-18, pp. 474-480.

[9] M. Kimura, N. Miyakoshi, and M. Diabow, "A miniature opto-electric transformer," in *Proc. IEEE Microelectromechanical Systems Workshop,* 1991, pp. 227–232.

[10] M. Mino, T. Yachi, A. Tago, K. Yanagisawa, and K. Sakakibara, "A new planar transformer for use in micro-switching converters," *IEEE Trans. Magn.,* vol. 28, pp. 1969–1973, July 1992.

[11] C. H. Ahn, Y. J. Kim, and M. G. Allen, "A fully integrated micromachined toroidal inductor with a nickel-iron magnetic core (switched dc/dc converter application)," in *Proc. Transducers, 6th Int. Conf. Solid-State Sensors and Actuators,* 1993, pp. 70–73.

[12] A. Olivei, "Optimized miniature thin-film planar inductors compatible with integrated circuits," *IEEE Trans. Parts, Mater., Packag.,* vol. PMP-5, no. 2, pp. 71–88, 1969.

[13] H. M. Greenhouse, "Design of planar rectangular microelectronic inductors," *IEEE Trans. Parts, Mater. Packag.,* vol. PMP-10, pp. 101–109, June 1974.

[14] R. Rodriguez, J. M. Dishman, F. D. Dickens, and E. W. Whelan, "Modeling of two-dimensional spiral inductors," *IEEE Trans. Comp., Hybrids, Manufact. Technol.,* vol. CHMT-3, pp. 535–541, Dec. 1980.

[15] W. A. Roshen and D. E. Turcotte, "Planar inductors on magnetic substrate," *IEEE Trans. Magn.,* vol. 24, pp. 3213–3216, Nov. 1988.

[16] O. Oshiro, H. Tsujimoto, and K. Shirae, "A novel miniature planar inductor," *IEEE Trans. Magn.,* vol. MAG-23, pp. 3759–3761, Sept. 1987.

[17] K. Kawabe, H. Koyama, and K. Shirae, "Planar inductors," *IEEE Trans. Magn.,* vol. MAG-20, pp. 1804–1806, 1984.

[18] M. Yamaguichi, M. Matsumoto, H. Ohzeki, and K. I. Arai, "Fabrication and basic characteristics of dry-etched micro inductors," *IEEE Trans. Magn.,* vol. 26, pp. 2014–2016, 1990.

[19] L. T. Romankiw, I. Croll, and M. Hatzaki, "Batch fabricated thin film magnetic recording heads," *IEEE Trans. Magn.,* vol. 6, pp. 579-599, May 1970.

[20] Y. Miura, T. Takahashi, F. Kume, J. Toda, S. Tsutsumi, and S. Kawakami, "Fabrication of multi-turn thin film head," *IEEE Trans. Magn.,* vol. MAG-16, pp. 779–881, Sept. 1980.

[21] Y. Noro, I. Ohshima, M. Saito, M. Yamada, and K. Tanaka, "Fabrication of multitrack thin-film head," *J. Appl. Phys.,* vol. 53, no. 3, pp. 2611–2613, Mar. 1982.

[22] M. Yamaguchi, "Characterization and analysis of a thin film charactor with closed magnetic circuit structure," *IEEE Trans. Magn.,* vol. 28, pp. 3015–3017, 1992.

[23] C. H. Ahn and M. G. Allen, "A planar micromachined spiral inductor for magnetic microactuator applications," *J. Micromech. Microeng.,* vol. 3, pp. 1–9, 1993.

[24] C. H. Ahn, Y. J. Kim, and M. G. Allen, "A fully integrated planar toroidal inductor with a micromachined nickel-iron bar," *IEEE Transactions Comp., Packag., Manufact. Technol.,* vol. 17, pp. 463–469, Sept. 1994.

[25] C. H. Ahn and M. G. Allen, "A new toroidal-meander type integrated inductor with a multilevel meander magnetic core," *IEEE Trans. Magn.,* vol. 30, pp. 73–79, Jan. 1994.

[26] R. L. Anderson, A. Gangulee, and L. T. Romankiw, "Annealing behavior of electroplated permalloy thin film," *J. Electron. Mater.,* vol. 2, no. 2, pp. 161-176, 1973.

[27] A. B. Frazier and M. G. Allen, "High aspect ratio electroplated microstructures using a photosensitive polyimide process," *IEEE J. Microelectromech. Syst.,* vol. 2, pp. 87–94, June 1993.

[28] A. B. Frazier, C. H. Ahn, and M. G. Allen, "Development of micromachined devices using polyimide-based processes," *Sens. Actuators,* vol. A-45, pp. 47–55, 1994.

[29] C. H. Ahn, "Micromachined components as integrated inductors and magnetic microactuators," Ph.D. dissertation, Dep. Elect. Comput. Eng., Georgia Inst. Technol., Atlanta, 1993.

[30] R. F. Soohoo, "Magnetic thin film inductors for integrated circuit application," *IEEE Trans. Magn.,* vol. MAG-15, pp. 1803–1805, Nov. 1979.

[31] S. Kawahito, Y. Sasaki, M. Ashiki, and T. Nakamura, "Micromachined solenoid for highly sensitive magnetic sensors," in *Proc. Transducers, 6th Int. Conf. Solid-State Sensors and Actuators,* San Francisco, CA, June 1991, pp. 1077–1080.

[32] R. Jensen, J. Cummings, and H. Vora, "Copper/polyimide materials system for high performance packaging," *IEEE Trans. Comp., Hybrids, Manufact. Technol.,* vol. 7, pp. 384–393, Dec. 1990.

[33] N. Iwasaki and S. Yamaguchi, "A pillar shaped via structure in a Cu-polyimide multilayer substrate," *IEEE Trans. Comp., Hybrids, Manufact. Technol.,,* vol. 13, pp. 440–443, no. 2, June 1990.

[34] I. W. Wolf, "Electrodeposition of magnetic materials," *J. Appl. Phys.,* vol. 33, no. 3, pp. 1152–1159, Mar. 1962.

[35] M. E. Henstock and E. S. Spencer-Timms, "The composition of thin electrodeposited alloy films with special reference to nickel-iron," in *Proc. 6th Int. Metal Finishing Conf.,* 1963, pp. 179–185.

[36] C. H. Ahn and M. G. Allen, "A fully integrated surface micromachined magnetic with a microactuator meander magnetic core," *IEEE J. Microelectromech. Syst.,* vol. 2, pp. 15–22, Mar. 1993.

[37] C. H. Ahn, Y. J. Kim, and M. G. Allen, "A planar variable reluctance magnetic micromotor with fully integrated stator and coils," *IEEE J. Microelectromech. Syst.,* vol. 2, pp. 165–173, Dec. 1993.

[38] C. H. Ahn and M. G. Allen, "Fluid micropumps based-on rotary magnetic actuators," in *Proc. IEEE Microelectromechanical Systems Workshop,* Amsterdam, The Netherlands, Jan. 30–Feb. 2, 1995, pp. 408-412.

[39] ——, "A comparison of two micromachined inductors for fully integrated boost DC/DC power converters," *IEEE Trans. Power Electron.,* vol.11, pp. 1-7, Mar. 1994.

[40] ——, "A fully integrated micromachined magnetic particle manipulator and separator," in *Proc. IEEE Microelectromechanical Systems Workshop,* Japan, Jan. 25–28, 1994, pp. 35-41.

Chong H. Ahn (S'90–M'91) received the Ph.D. degree in electrical and computer engineering (major in MEMS) from Georgia Institute of Technology, Atlanta, in 1993.

From 1993 through 1994, he was a Post-Doctoral Associate at Georgia Institute of Technology and then at IBM T. J. Watson Research Center. In 1994, he joined the Department of Electrical and Computer Engineering and Computer Science, University of Cincinnati, Cincinnati, OH, as an Assistant Professor. He is currently an Associate Professor. He is also an Associate Director of the Center for Microelectronic Sensors and MEMS (CMSM) at the University of Cincinnati. His research activities include magnetic microsensors and microactuators, microinductors and transformers, microfluidic systems, and bio/chemical detection systems. He has published 60 journal and conference papers related to MEMS and is the holder of three U.S. patents. He heads the Cincinnati Chapter of the Electrochemical Society. In addition, he is currently organizing, as Co-Chair, the SPIE International Conference on Microfluidic Devices and Systems and the Electrochemical Society Fifth International Symposium on Magnetic Materials, Processes and Devices.

Mark G. Allen (M'89) received the B.A. degree in chemistry, the B.S.E. degree in chemical engineering, and the B.S.E degree in electrical engineering from the University of Pennsylvania, Philadelphia, in 1984 and the S.M. and Ph.D. degrees from Massachusetts Institute of Technology, Cambridge, in 1986 and 1989, respectively.

In 1989, he joined the faculty of the School of Electrical and Computer Engineering, Georgia Institute of Technology, Atlanta, where he is currently an Associate Professor. His research area is micromachining, with special emphasis on magnetic materials and devices, micromachining issues in electronic packaging, and micromachined fluidic devices.